

Ferroelectric properties and dynamic scaling of 100 oriented (K 0.5 Na 0.5) NbO 3 single crystals

Shashaank Gupta and Shashank Priya

Citation: [Applied Physics Letters](#) **98**, 242906 (2011); doi: 10.1063/1.3600058

View online: <http://dx.doi.org/10.1063/1.3600058>

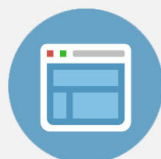
View Table of Contents: <http://scitation.aip.org/content/aip/journal/apl/98/24?ver=pdfcov>

Published by the [AIP Publishing](#)



Re-register for Table of Content Alerts

Create a profile.



Sign up today!



Ferroelectric properties and dynamic scaling of $\langle 100 \rangle$ oriented $(\text{K}_{0.5}\text{Na}_{0.5})\text{NbO}_3$ single crystals

Shashaank Gupta and Shashank Priya^{a)}

Center for Energy Harvesting Materials and Systems (CEHMS), Virginia Tech, Blacksburg, Virginia 24061, USA

(Received 19 March 2011; accepted 24 May 2011; published online 17 June 2011)

In this letter, we report the dielectric and ferroelectric (FE) characteristics of potassium sodium niobate ($\text{K}_{0.5}\text{Na}_{0.5}\text{NbO}_3$) single crystals grown by flux method. Orientation analysis of as-grown cubical-shaped crystals was conducted by electron backscattered diffraction technique revealing the $\langle 100 \rangle$ crystallographic orientation of two opposing major faces. Annealed crystals were found to exhibit FE orthorhombic to FE tetragonal transition temperature of 200 °C and Curie temperature of 407 °C. Poled $\langle 100 \rangle$ oriented crystals had longitudinal piezoelectric constant of 148 pC/N. Dielectric measurement as a function of temperature was conducted to determine the second order parameter in Gibbs free energy expansion. Dynamic hysteresis analysis on these crystals showed the power law relations to be of the form $\langle A \rangle \propto f^{0.47} E_o^{-0.85} E_o^{1.45} f^{0.14}$ and $\langle A \rangle \propto f^{0.04} E_o$ below and above the coercive field. © 2011 American Institute of Physics. [doi:10.1063/1.3600058]

Potassium sodium niobate ($\text{K}_{0.5}\text{Na}_{0.5}\text{NbO}_3$) abbreviated as KNN, is one of the potential candidates for lead-free piezoelectric material. Since the properties of random polycrystalline KNN ceramic are inferior to that of $\text{Pb}(\text{Zr},\text{Ti})\text{O}_3$ (PZT), research has focused on development of textured KNN ceramic and cost-effective KNN single crystals by using flux method.^{1,2} Textured ceramic samples of modified KNN compositions have shown promising improvement in electrical properties,^{3,4} though single crystal still lacks the expected ferroelectric and piezoelectric properties. Kizaki *et al.*¹ have reported the synthesis of KNN single crystals by flux method but due to high conductivity they were not successful in measuring piezoelectric properties. Even annealing the KNN crystals in air and oxygen did not result in significant improvement in resistivity. An increase in resistivity was achieved by doping small amount of Mn (Ref. 1) and remanent polarization was found to be about 40 $\mu\text{C}/\text{cm}^2$. Recently Lin *et al.*² have showed that improvement in piezoelectric properties of KNN single crystals by Mn doping was due to the presence of higher domain density (lower domain size).

In this letter, we report the piezoelectric and dynamic ferroelectric characteristics of large size pure KNN single crystals. The procedure for crystal growth is as follows. Calcined KNN powder was mixed with salts NaF and KF in the ratio of 10:3:2 and ball milled for 6 h. After drying, this solution was loaded in a platinum crucible and rapidly heated to 1080 °C for 2 h. The blue colored cubical shaped crystals were grown uniformly in the crucible with maximum size of 5 mm \times 5 mm \times 2 mm. X-ray diffraction analysis confirmed the orthorhombic phase and (100) orientation. X-ray photoelectron spectroscopic analysis conducted on the as-grown crystal showed its composition to be $\text{K}_{0.49}\text{Na}_{0.51}\text{NbO}_3$. Orientation analysis was conducted to confirm the crystallographic orientation of two opposite faces of these crystals by electron backscattered diffraction analysis. Figure 1 shows the indexed Kikuchi pattern obtained for one of the faces.

Indexed Kikuchi pattern provided Euler's angles to be (238°, 93°, and 181°) and corresponding crystallographic orientation of crystal is shown in inset of figure. Similar values of Euler's angles were found for opposite face of crystal suggesting that these two faces were parallel and exhibited (100) orientation.

As grown crystals had high leakage and could not be poled. This high leakage current can be attributed to the presence of oxygen ion vacancies¹ in the lattice and composition of as-grown crystals could be represented as $\text{K}_{0.5}\text{Na}_{0.5}\text{NbO}_{3-\delta}$. Blue color of these crystals also supports this argument which is generally associated with oxygen vacancies in perovskites.¹ The missing oxygen ions give rise to $2e^-$ in the conduction band according to Eq. (1) and hence result in low resistivity,⁵



Annealing these crystals in air at 850 °C helped in compensating the oxygen vacancies and the color was changed

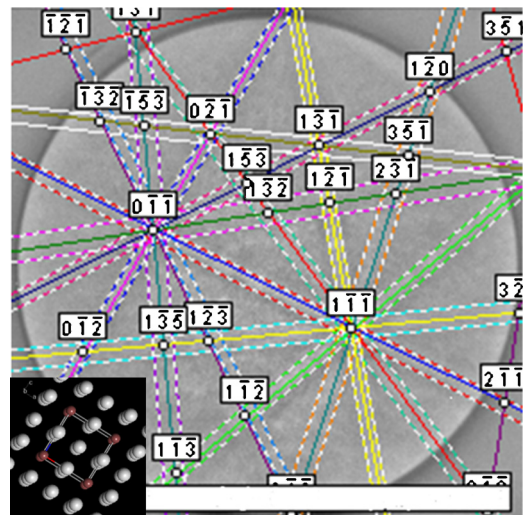


FIG. 1. (Color online) Electron backscattered diffraction pattern obtained on one of the faces of KNN crystal. Inset of the figure shows the corresponding crystallographic orientation of the crystal.

^{a)}Electronic mail: spriya@vt.edu.

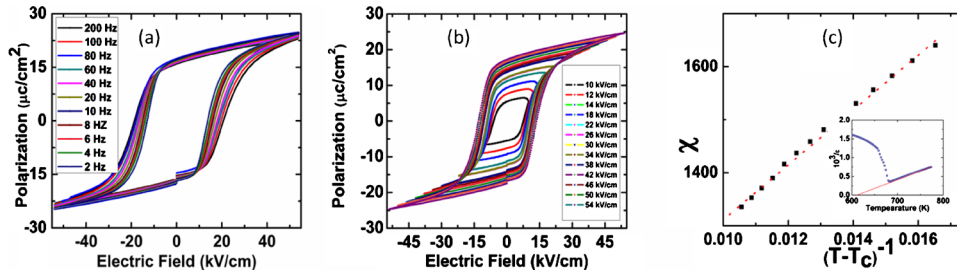


FIG. 2. (Color online) Hysteresis loops obtained for (100) oriented KNN single crystals, (a) varying frequencies at applied field of 54 kV/cm, (b) varying electric fields at frequency of 2 Hz, and (c) variation in dielectric susceptibility with $1/(T-T_c)$ at $T > T_c$ gives the value of Curie constant to be 4.2×10^4 K. Inset of figure shows the $10^3/\epsilon$ vs T plot.

from blue to transparent. At 100 kHz, annealed crystals were found to possess ac resistivity magnitude of $1.17 \times 10^4 \Omega \text{ m}$ in contrast to $1.32 \times 10^2 \Omega \text{ m}$ before annealing. Activation energies calculated from impedance spectroscopy for these crystals were found to be 1.3 eV and 1.2 eV respectively before and after annealing. These values are consistent with the reported activation energy for oxygen ion conduction in perovskites.^{6,7}

Dielectric response as a function of temperature was measured to identify the Curie temperature ($T_c \sim 407^\circ \text{C}$) and orthorhombic to tetragonal transition temperature ($T_{o-t} \sim 200^\circ \text{C}$). At room temperature dielectric constant and loss values were found to be 226 and 0.08, consistent with the inherent low permittivity of KNN.⁸ For piezoelectric measurements crystals were poled at 3 kV/mm at 130°C . Low field longitudinal piezoelectric coefficient (d_{33}) value was measured to be 148 pC/N. Figures 2(a) and 2(b) shows the saturated ferroelectric hysteresis loops obtained on KNN crystals exhibiting remnant polarization (P_r) and coercive field (E_c) values of $18 \mu\text{C}/\text{cm}^2$ and 20 kV/cm. It can be seen that ferroelectric loops are square shaped, even below the coercive field. Landau–Devonshire (L–D) theory was used to correlate dielectric stiffness to the shape of ferroelectric loops. According to L–D theory,^{9,10} Gibbs free energy function can be written as follows: $G = (1/2)\alpha P^2 + (1/4)\beta P^4 + (1/6)\gamma P^6 - EP$. Neglecting the higher order terms, this equation can be reduced to $E = \alpha P$, where $\alpha = T_c - T_o / \epsilon_o C$, and C is the Curie constant. Curie constant can be calculated by plotting the dielectric susceptibility as a function of $1/(T-T_c)$ according to the equation $\chi = C/(T-T_c)$, $T > T_c$. Figure 2(c) shows the plot of susceptibility χ versus $1/(T-T_c)$ providing the magnitude of Curie constant to be 4.2×10^4 K. Inset of figure shows the variation of $10^3/\epsilon$ versus T , and by extending the linear part the magnitude of T_o was found to be 636 K. Using these values, the magnitude of α was found to be 1.1×10^8 m/F. According to Landau–Khalatnikov simulation, which is a dynamic version of L–D theory, the parameter α is measure of shape of ferroelectric loops and its higher magnitude leads to square shaped ferroelectric loops.¹¹ The value of α obtained for KNN single crystals is on the higher side and accounts for the square shape of ferroelectric loops.^{10,11}

The ferroelectric response of the pure crystals was lower than that expected for the (100) oriented orthorhombic phase. In order to understand this observation, dynamic hysteresis analysis based on $(\Phi^2)^2$ model was conducted on these crystals. Originally this model was established for magnetic materials using Heisenberg model based on nonequilibrium statistical mechanical theory but can be applied equally well to ferroelectrics as domain reversal dynamics have similarity in two cases.^{12–15} Dynamic hysteresis analysis relates the area under the ferroelectric loop $\langle A \rangle$ to the amplitude (E_o)

and frequency (f) of applied electric field, according to power law relation $\langle A \rangle \propto f^m E_o^n$,^{16,17} where the parameters m and n are mainly controlled by domain states and polarization switching mechanism. Theoretical calculations based on $(\Phi^2)^2$ model suggest the values of m and n to be -1 and 2 , respectively, for high frequencies and $1/3$ and $2/3$ for low frequencies.^{12,18} Experimentally it has been observed that the frequency (f_c) at which the equation $\langle A \rangle \propto f^m E_o^n$ flips from one set of exponents to others, also depends upon applied electric field and increases with increase in applied electric field.¹⁹ The exponent m in this relation refers to switching time required by the domains at a given electric field. Its value is governed by charge defects and space charge present in the sample and higher negative value means higher response time of domains. On the other hand, the exponent of electric field n is a measure of ability of domains by which they respond to change in electric field direction.²⁰ Higher value of n means sharper response of domains and hence higher value of polarization.²¹

Ferroelectric loops were obtained for electric fields varying from 10 to 54 kV/cm while frequency range covered during measurement was 2–200 Hz. Figures 2(a) and 2(b) show the ferroelectric loops obtained at different f but fixed E_o (54 kV/cm) and different E_o but fixed frequency ($f = 2$ Hz). Similar loops were obtained for other possible combinations of E_o and f and the area under the loop ($\langle A \rangle$) was calculated. Figures 3(a) and 3(b) show the variation of hysteresis loop area with frequency (at different electric fields) and electric field (at different frequencies), respectively. If we carefully observe the Fig. 3(a), the area of the curves obtained for $E_o < 20$ kV/cm decreases with increasing frequency while for $E_o > 20$ kV/cm reverse effect was observed. On the other hand, Fig. 3(b) shows that in the whole frequency range the area under the loop $\langle A \rangle$ increases monotonically with applied electric field, though the rate of increase in $\langle A \rangle$ with E_o is higher for higher frequencies.

To obtain the value of m , i.e., the exponent expressing the variation in $\langle A \rangle$ with frequency, each of the plot in Fig. 3(a) was fitted to the equation $\langle A \rangle \propto f^m$. Different values of m

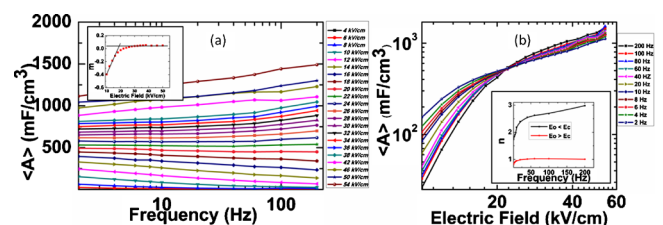


FIG. 3. (Color online) Variation in area $\langle A \rangle$ under ferroelectric loop (a) with frequency, at different E_o values, and (b) with electric field at different applied frequencies. Inset of the two figures show variations in the values of exponent m and n , respectively.

obtained for different electric fields are plotted in the inset of same figure. Clearly the plot can be divided into two parts, first with $E_o < 20$ kV/cm and other having $E_o > 20$ kV/cm. Except for the electric field range where two linear regions coincide ($E_o \sim 20$ kV/cm), fitting to the curves was excellent ($R^2 > 0.97$). Though generally the coercive field is frequency dependent, in our case where m versus E_o plot is changing its slope, can be considered as coercive field ($E_c = 20$ kV/cm). The two linear regions were further fitted to obtain the variation in m with applied electric field. It was found that for $E_o < E_c$, $m = 0.47E_o - 0.85$ ($R^2 > 0.97$) and field independent values of m was 0.04 ($R^2 > 0.90$) for $E_o > E_c$. Similarly, $\langle A \rangle$ versus electric field curves in Fig. 3(b) were fitted for different frequencies to obtain the value of n according to the relation $\langle A \rangle \propto E_o^n$. Again the data in Fig. 3(b) can be partitioned in two parts, one for $E_o < E_c$ and other having $E_o > E_c$. Values of n obtained by fitting the curves for different frequencies ($R^2 > 0.97$) are shown in the inset of Fig. 3(b) and are frequency dependent. These data points are further fitted to obtain the frequency dependence of exponent n . For $E_o < E_c$, $n = 1.45^* f^{0.14}$ ($R^2 > 0.99$) and for $E_o > E_c$, $n = 1 - 0.25^* \exp(-0.13f)$ ($R^2 > 0.98$). This value of n is complex but it can be seen that at $f > 10$ Hz it is almost constant and equal to 1.

Hence, the power law relations for $E_o < E_c$ and $E_o > E_c$ can be expressed by Eq. (2) as follows:

$$\langle A \rangle \propto f^{0.47E_o - 0.85} E_o^{1.45f^{0.14}} \quad E_o < E_c,$$

$$\langle A \rangle \propto f^{0.04} E_o \quad E_o > E_c. \quad (2)$$

It can be clearly seen from these equations that the values of m and n are pretty complex for $E_o < E_c$ and do not match with theoretically predicted values by $(\Phi^2)^2$ and $(\Phi^2)^3$ models.^{12,18} Also the scaling behavior of minor loops is completely different from saturated loops. This kind of behavior is related to variation in response of domains below and above coercive field.

The domains responding below the average coercive field of crystals are small in size and known as reversible domains.¹⁵ On the other hand the irreversible domains are comparatively larger and respond at fields higher than E_c . In the case of relaxors, the nonlinear hysteretic response below the coercive field is well-known phenomenon. Unpoled relaxor is a glassy state, however, polarization irregularities are known to exist within a poled condition in the vicinity of randomly quenched defects. We anticipate a multi-polar state exists in the KNN crystal under the applied field due to polymorphic transition from orthorhombic to tetragonal symmetry. For minor loops, electric field dependence of exponent m is similar to that observed for conventional ferroelectric such as BaTiO₃ single crystals.¹⁷ The value of exponent n remains greater than 2 for most of the frequency range suggesting ease of domains in responding to changes in applied electric field direction. These values for m and n imply that for minor loops, $\langle A \rangle$ decays more slowly with f and increases much faster with E_o , as compared to theoretical predictions for magnetic materials.¹² This observation can be attributed to the fact that reversible domains responding to $E_o < E_c$, are kinetically easier to switch and hence less sensitive to frequency and more sensitive to field.¹⁵ In case of $E_o > E_c$, m is almost independent of electric field with value close to zero.

Hence the area of saturated loops is independent of frequency of applied field. The value of exponent n , which is constant at 1 for $f > 8$ Hz, is lower than theoretically predicted value of 2. Since the value of exponent n is the measure of ability of domains in following the electric field direction, lower value indicates poor ability of irreversible domains in this respect.²¹ As a consequence, the lower value of n leads to lower hysteresis area as well as lower value of remnant polarization.¹⁶ Also the near linear dependence of $\langle A \rangle$ to electric field also suggests occurrence of concurrent nucleation and domain boundary motion, phenomena very well known in KNbO₃ and BaTiO₃.²² Linear electric field dependence of parameter m at sub-coercive fields and simultaneous nucleation of irreversible domain with domain boundary motion show KNN resembles BaTiO₃ in dynamic scaling.

In summary, KNN single crystals were grown by flux method. Dynamic scaling analysis provided relationships of the form: $\langle A \rangle \propto f^{0.47E_o - 0.85} E_o^{1.45f^{0.14}}$ and $\langle A \rangle \propto f^{0.04} E_o$ for $E_o < E_c$ and $E_o > E_c$, respectively. Poor ferroelectric nature of these crystals can be attributed to lower value of exponent n for saturated loops.

The authors gratefully acknowledge the financial support from Office of Basic Energy Science, Department of Energy (Grant No. DE-FG02-07ER6480).

¹Y. Kizaki, Y. Noguchi, and M. Miyayama, *Appl. Phys. Lett.* **89**, 142910 (2006).

²D. Lin, Z. Li, S. Zhang, Z. Xu, and X. Yao, *J. Am. Ceram. Soc.* **93**, 941 (2010).

³Y. Saito, H. Takao, T. Tani, T. Nonoyama, K. Takatori, T. Homma, T. Nagaya, and M. Nakamura, *Nature (London)* **432**, 84 (2004).

⁴Y. Chang, S. F. Poterala, Z. Yang, S. Trolier-McKinstry, and G. L. Messing, *Appl. Phys. Lett.* **95**, 232905 (2009).

⁵H. Y. Hwang, *Nature Mater.* **4**, 803 (2005).

⁶K. W. Browall, O. Muller, and R. H. Doremus, *Mater. Res. Bull.* **11**, 1475 (1976).

⁷T. L. Nguyen, M. Dokiya, S. Wang, H. Tagawa, and T. Hashimoto, *Solid State Ionics* **130**, 229 (2000).

⁸L. Egerton and D. M. Dillon, *J. Am. Ceram. Soc.* **42**, 438 (1959).

⁹K. M. Rabe, C. H. Ahn, and J.-M. Triscone, *Physics of Ferroelectrics: A Modern Perspective* (Springer, New York, 2007).

¹⁰D. Maurya, N. Wongdamnern, R. Yimnirun, and S. Priya, *J. Appl. Phys.* **108**, 124111 (2010).

¹¹T. K. Song, *J. Korean Phys. Soc.* **46**, 5 (2005).

¹²M. Rao, H. R. Krishnamurthy, and R. Pandit, *Phys. Rev. B* **42**, 856 (1990).

¹³M. Rao and R. Pandit, *Phys. Rev. B* **43**, 3373 (1991).

¹⁴M. Rao, H. R. Krishnamurthy, and R. Pandit, *J. Appl. Phys.* **67**, 5451 (1990).

¹⁵Y. Y. Guo, T. Wei, Q. Y. He, and J.-M. Liu, *J. Phys.: Condens. Matter* **21**, 485901 (2009).

¹⁶R. Yimnirun, Y. Laosiritaworn, S. Wongsanmai, and S. Ananta, *Appl. Phys. Lett.* **89**, 162901 (2006).

¹⁷N. Wongdamnern, A. Ngamjarrojana, Y. Laosiritaworn, S. Ananta, and R. Yimnirun, *J. Appl. Phys.* **105**, 044109 (2009).

¹⁸M. Acharyya and B. K. Chakrabarti, *Phys. Rev. B* **52**, 6550 (1995).

¹⁹B. Pan, H. Yu, D. Wu, X. H. Zhou, and J.-M. Liu, *Appl. Phys. Lett.* **83**, 1406 (2003).

²⁰N. Wongdamnern, A. Ngamjarrojana, S. Ananta, Y. Laosiritaworn, and R. Yimnirun, *Key Eng. Mater.* **421-422**, 399 (2010).

²¹N. Wongdamnern, N. Triamnak, M. Unruan, K. Kanchiang, A. Ngamjarrojana, S. Ananta, Y. Laosiritaworn, and R. Yimnirun, *Phys. Lett. A* **374**, 391 (2010).

²²J. M. Liu, H. L. W. Chan, C. L. Choy, and C. K. Ong, *Phys. Rev. B* **65**, 014416 (2001).